Simultaneous imaging of ultrasound attenuation, speed of sound and optical absorption in a photoacoustic setup

Rene G.H. Willemink[a], Srirang Manohar[b], Jithin Jose[b], Kees Slump[a], Ferdi van der Heijden[a] and Ton G. van Leeuwen[b]

[a]University of Twente, Signals and Systems Group, P.O. Box 217 7500AE, Enschede, the Netherlands;

[b]University of Twente, Biophysical Engineering Group, P.O. Box 217 7500AE, Enschede, the Netherlands

ABSTRACT

Photoacoustic imaging is a relatively new medical imaging modality. In principle it can be used to image the optical absorption distribution of an object by measurements of optically induced acoustic signals. Recently we have developed a modified photoacoustic measurement system which can be used to simultaneously image the ultrasound propagation parameters as well. By proper placement of a passive element we obtain isolated measurements of the object's ultrasound propagation parameters, independent of the optical absorption inside the object. This passive element acts as a photoacoustic source and measurements are obtained by allowing the generated ultrasound signal to propagate through the object. Images of the ultrasound propagation parameters, being the attenuation and speed of sound, can then be reconstructed by inversion of a measurement model. This measurement model relates the projections non-linearly to the unknown images, due to ray refraction effects. After estimating the speed of sound and attenuation distribution, the optical absorption distribution is reconstructed. In this reconstruction problem we take into account the previously estimated speed of sound distribution. So far, the reconstruction algorithms have been tested using computer simulations. The method has been compared with existing algorithms and good results have been obtained.

Keywords: photoacoustic imaging, ultrasound tomography, inhomogeneous speed of sound, ray refraction correction

1. INTRODUCTION

Photoacoustic (PA) imaging is a relatively new imaging technique, which primarily focuses on the reconstruction of optical properties of the imaged object. The technique is well suited for medical imaging purposes due to its noninvasive character and its ability to penetrate through soft tissue. Photoacoustic imaging is based on the generation of acoustic waves due to the absorption of optical energy. A good overview of photoacoustic imaging can be found in the article of Xu and Wang.[1]

The reconstruction of optical properties of the imaged object is based on the measurements of ultrasound signals. These ultrasound signals originate from inside the imaged object and have been induced by an external light source. When the light source emits a short pulse of light, an initial pressure distribution will result in the imaged object. The magnitude of the initial pressure distribution is proportional to the optical energy absorption distribution.[2] The generated pressure distribution will propagate outwards through the object and can be measured by ultrasound transducers. Since the generated acoustic signals travel through the object, the received signals are not only dependent on the optical properties but also on the acoustic properties of the object. In most of the existing photoacoustic reconstruction algorithms, the acoustic properties are assumed to be homogeneously distributed. Objects which do not satisfy this homogeneity can not be accurately reconstructed with these algorithms and result in blurred and artifacted images.

Several authors have considered the incorporation of speed of sound inhomogeneities in the reconstruction process. These methods can be divided into methods which require an a priori known speed of sound map and methods without this requirement.

Further author information: (Send correspondence to Rene Willemink)
Rene Willemink: E-mail: rene.willemink@utwente.nl

Medical Imaging 2009: Ultrasonic Imaging and Signal Processing, edited by Stephen A. McAleavey, Jan D'hooge
Proc. of SPIE Vol. 7265, 72650J · © 2009 SPIE · CCC code: 1605-7422/09/$18 · doi: 10.1117/12.810905

1.1 Algorithms which require an a priori known speed of sound map

Anastasio et al[3] demonstrated the reconstruction of photoacoustic measurements by assuming an a priori known speed of sound map. Using this speed of sound map, curved iso-time of flight (TOF) contours were calculated by assuming straight ray propagation of speed of sound. The photoacoustic measurement function, valid for homogeneous speed of sound distributions was modified to include inhomogeneous speed of sound distributions by specifying the integration over the curved iso-TOF contours instead of circles. The reconstruction was then accomplished by solving the positive linear photoacoustic measurement equation by using an EM-algorithm.

Jin[4] used a similar approach. The speed of sound map in this case was pre-calculated by performing a separate ultrasound transmission tomography (UTT) step. Here linear ray paths are assumed so that a filtered back projection reconstruction can be used in the UTT step. Curved iso-TOF contours were then calculated using the same algorithm as Anastasio,[3] i.e. by assuming straight ray sound propagation. The inversion of the linear photoacoustic measurement equation was then performed by directly using the iterative LSQR method.[5]

1.2 Algorithms which do not require an a priori known speed of sound map

Jiang et al[6] used a finite element discretized version of an inhomogeneous acoustic wave equation in the frequency domain. In the wave equation, terms representing the optical absorption distribution, acoustic property distributions and generated pressure are present. This results in a non-linear system of equations involving the unknown optical absorption and acoustic property distributions and the known pressure which is measured at the boundary of the imaging domain. The reconstruction algorithm is then implemented by iteratively solving a linearized system of equations. The linearization is done by calculating a first order taylor expansion with respect to the unknown optical absorption and acoustic property distributions.

Jin Zhang et al[7] use the same photoacoustic measurement function as Anastasio[3] to relate the optical absorption distribution and curved iso-TOF contours to the measured ultrasound signals. The speed of sound distribution was not assumed to be known a priori, however a low dimensional parametrization was used. This parametrization allows the speed of sound distribution to be represented by a limited number of predefined areas with unknown constant speed of sound values. The actual values of the predefined areas are a priori unknown, but their boundaries are assumed to be known. A cost function was formulated that minimizes the difference between predicted and observed measurements and penalizes the roughness of the reconstructed speed of sound and optical absorption distributions. The nonlinear cost function was minimized by iteratively switching between solving for the speed of sound distribution with constant optical absorption and solving for the optical absorption distribution with constant speed of sound. In the first step, with constant optical absorption, a gradient descent step was performed where the direction of the cost function gradient was calculated numerically. In the second step, with constant speed of sound, a quadratic cost function is obtained which was solved using a conjugate gradient method.

Chi Zhang and Wang[8] also propose a method which does not assume any speed of sound distribution to be known a priori. In this method, curved iso-TOF contours are used again in the formulation of the photoacoustic measurement model. However, the calculation of these iso-TOF contours is completely different and does not involve tracing rays through an intermediate speed of sound distribution. Instead, the correlation between integrated photoacoustic signals from origin symmetric detector pairs is used. In the derivation of this method, several approximations were used which mainly involve the assumption that the imaged object is small or equivalently that the detectors are far away from the imaged object. Also, the speed of sound inhomogeneities should not be too high. The approach comes down to calculating a constant speed for each projection. Projections from origin symmetric detector pairs will share the same speed of sound.

2. APPROACH

Our approach is based on a single step photoacoustic measurement which allows for simultaneous and independent reconstruction of the acoustic properties and optical absorption distribution. Both the speed of sound and acoustic attenuation distributions can in principle be reconstructed. Our setup consists of a modified conventional circular photoacoustic scanning system. By adding an extra, carefully positioned, passive element to our setup that converts a part of the incident optical energy into acoustic energy in the form of a short acoustic pulse,

we can obtain isolated measurements of the object's acoustic properties. By doing this, we have effectively created a measurement setup with can generate UTT and photoacoustic measurements simultaneously using only optical input energy. More information about our photoacoustic measurement setup can be found in previous publications.[9–11]

2.1 Photoacoustic wave propagation

The propagation of photoacoustic pressure waves in inhomogeneous speed of sound media, is governed by the following partial differential equation:[4]

$$\nabla^2 p(\boldsymbol{r},t) - \frac{1}{c^2(\boldsymbol{r})}\frac{\partial^2 p(\boldsymbol{r},t)}{\partial t^2} = -\frac{\beta}{C_p}\frac{\partial I(t)}{\partial t}A(\boldsymbol{r}) \tag{1}$$

Here, β is the volume thermal expansion coefficient, C_p is the specific heat, $p(\boldsymbol{r},t)$ is the generated pressure at location $\boldsymbol{r}$ and time t, $c(\boldsymbol{r})$ is the acoustic speed distribution, $I(t)$ is the laser pulse profile and $A(\boldsymbol{r})$ is the optical absorption distribution. A solution to this wave equation can be found for the constant speed case. The illumination function of the laser $I(t)$ will be seen as a delta pulse. In the case of an inhomogeneous speed of sound distribution, an approximate solution can be found as:[12]

$$p(\boldsymbol{r},t) = \eta\frac{\partial}{\partial t}\iint\limits_{t=t_f(\boldsymbol{r}',\boldsymbol{r})}\frac{A(\boldsymbol{r}')}{|\boldsymbol{r}-\boldsymbol{r}'|}\mathrm{d}\boldsymbol{r}' \tag{2}$$

where η is a constant and $t_f(\boldsymbol{r}',\boldsymbol{r})$ is the TOF for a pressure wave to travel from point $\boldsymbol{r}$ to point $\boldsymbol{r}'$. This function is dependent on the speed of sound distribution $c(\boldsymbol{r})$. Relation (2) shows that the generated pressure can be seen as the projections over iso-TOF contours, which are determined by the TOF function $t_f(\boldsymbol{r}',\boldsymbol{r})$. From this relation, we can see that given a speed of sound distribution, the relation between optical absorption $A(\boldsymbol{r})$ and the measured pressure $p(\boldsymbol{r},t)$ is linear. This relation has been used by the authors of other SOS compensated photoacoustic reconstruction[3,4,7,8] methods. Their approaches differ in the way that the TOF function is calculated. The first three authors use a ray integral over the speed of sound distribution:

$$t_f(\boldsymbol{r}',\boldsymbol{r}) = \int_{l(\boldsymbol{r}',\boldsymbol{r})}\frac{1}{c(\boldsymbol{r}'')}\mathrm{d}\boldsymbol{r}'' \tag{3}$$

where the ray path is the straight line connecting $\boldsymbol{r}'$ and $\boldsymbol{r}$ directly. An other approach was used by Chi Zhang and Wang,[8] which calculate the function based on the cross correlation between received signals of two opposite detector pairs:

$$t_f(\boldsymbol{r}',\boldsymbol{r}) = \frac{|\boldsymbol{r}'-\boldsymbol{r}|}{2|\boldsymbol{r}|}\arg\max_t R(\boldsymbol{r},t) \tag{4}$$

here $R(\boldsymbol{r},t)$ is the cross correlation function between the integrated measured signals of the detector at position $\boldsymbol{r}$ and the symmetrically opposite detector $-\boldsymbol{r}$.

We propose a different approach to calculate the TOF values, which takes refraction of rays into account. Our approach is based on solving the Eikonal equation:

$$|\nabla t(\boldsymbol{r})|^2 = \frac{1}{c(\boldsymbol{r})^2} \tag{5}$$

The Eikonal equation can be used to model acoustic wave front propagation with inhomogeneous speed of sound distributions. A computationable efficient method for calculation of the first arrival time solution to this equation can be obtained via the fast marching method (FMM).[13] The effectiveness of the FMM method to incorporate refraction of rays has already been demonstrated in the application area of UTT by Li et al.[14,15]

2.2 Reconstructing the optical absorption distribution

We outline here our method to reconstruct the optical absorption distribution $A(\boldsymbol{r})$ from a given number of pressure measurements $p(\boldsymbol{r}, t)$, obtained at different positions $\{\boldsymbol{r}_1, \ldots, \boldsymbol{r}_n\}$ at the outside of the object. The input measurements are sampled in the time domain with a certain sampling frequency. We represent the pressure measurements obtained at $\boldsymbol{r}_i$ in the measurement vector $\boldsymbol{z}_{\mathrm{p},i}$. So that we can construct a complete vector with measurements $\boldsymbol{z}_{\mathrm{p}} = [\boldsymbol{z}_{\mathrm{p},1}^T \ldots \boldsymbol{z}_{\mathrm{p},n}^T]^T$. The continuous optical absorption distribution $A(\boldsymbol{r})$ will be represented in our approach as a uniform sampled rectangular grid. We store this discrete representation of the optical absorption distribution in the vector $\boldsymbol{x}_{\mathrm{A}}$. Each element in the vector corresponds to a different node in the grid in the optical absorption distribution.

If we know, for each detector position, the corresponding TOF values at each of the grid points in $A(\boldsymbol{r})$, the forward model can be written as a specific sum of elements in $\boldsymbol{x}_{\mathrm{A}}$ followed by a differentiation operation. In matrix calculations, we write the discretized relation between all measurements and the unknown optical absorption map as:

$$\boldsymbol{z}_{\mathrm{p}} = \mathrm{H}_{\mathrm{dt}}\mathrm{H}_{\mathrm{TOF}}\boldsymbol{x}_{\mathrm{A}} \tag{6}$$

where H_{dt} is a large and sparse matrix which represents the time derivative and $\mathrm{H}_{\mathrm{TOF}}$ is a large and sparse matrix which represents the integral. Reconstructing the optical absorption map can now be performed by calculating a solution to this linear system of equations. Because the number of equations and unknowns in this problem is very large, the solution to this problem has to be found with an iterative method, since a direct method takes too much time to compute. There are several methods to solve this problem. Anastasio et al[3] use an EM algorithm, Jin and Wang[4] use LSQR, Jin Zhang et al[7] use a truncated conjugate gradient (TCG) method with a roughness penalty and Chi Zhang and Wang[8] use a modified filtered back projection (FBP) applied over the iso-TOF curves. We have chosen to use the LSQR algorithm in the reconstruction. The implementation of the EM algorithm needs more iterations.[3] The LSQR and TCG algorithm (applied to the normal equations) gave exactly the same results, however, the LSQR method is known to possess more favorable numerical properties.[5] We did not consider the modified FBP since this is an approximation which results in less accurate reconstructions.

By solving the system without regularization, i.e. without including any other information than just the measurements, artifacts can occur in the reconstruction. This happens when the forward model can not be uniquely solved. Situations where this can occur is when the measurements have noise and when the system is not overdetermined or maybe even underdetermined. A simple regularization by constraining the smoothness of the solution can really improve the reconstruction result. We have applied a regularization by adding the gradient of the reconstructed image in the cost function:

$$\hat{\boldsymbol{x}}_{\mathrm{A}} = \arg\min_{\boldsymbol{x}} \left(||\boldsymbol{z}_{\mathrm{p}} - \mathrm{H}_{\mathrm{dt}}\mathrm{H}_{\mathrm{TOF}}\boldsymbol{x}_{\mathrm{A}}||^2 + \lambda||\mathrm{H}_{\mathrm{Gx}}\boldsymbol{x}_{\mathrm{A}}||^2 + \lambda||\mathrm{H}_{\mathrm{Gy}}\boldsymbol{x}_{\mathrm{A}}||^2 \right) \tag{7}$$

Here H_{Gx} and H_{Gy} are sparse matrices that represent the gradient of the optical absorption distribution in the x and y direction respectively. The parameter λ controls the amount of smoothness we want in our solution. It selects the trade off between the mismatch of the observed and predicted measurements and the smoothness of the image. In statistical terms the λ parameter can be interpreted as the ratio between the expected variance of the measurement noise and the expected variance of the smoothness 'noise'.

It is important to consider the correct way to calculate the gradient matrices H_{Gx} and H_{Gy}. A second order accurate central difference scheme might seem a good choice, however, this can result in saw tooth artifacts in the reconstruction and therefor it should not be used. This is caused by the fact that the central difference does not consider the central point and only the two neighboring points. A first order forward or backward difference scheme results does not suffer from these artifacts, so that is the implementation we apply.

2.3 Calculating the TOF values

For each detector position, TOF values have to be calculated for each of the points in the grid. As explained before, we will use the first arrival time solution to the Eikonal equation to obtain these TOF values using the FMM[13] method.

The FMM method is an algorithm that solves the Eikonal equation in a single pass using upwind finite differences. We have implemented the high accuracy FMM (HAFMM) which uses second order accurate approximations to the gradient. When a good initialization is used, the numerical errors that occur in the solution are very small. The grid that we will use to represent the TOF values will enclose the same area as the optical absorption map, but does not need to have a the same grid spacing (it can be coarser). The grid is the same as the grid in which we know the speed of sound distribution. In this section we assume that this speed of sound distribution is known and in the next section we will see how we obtain this distribution.

We initialize the FMM method by assuming that the speed of sound outside the defined speed of sound grid has a constant and known value. The boundaries of the TOF grid which are in sight from the detector position are then initialized by assuming we can calculate it directly simply from the distance to the detector and the background speed of sound value. The in sight boundary grid points and their direct neighbor grid points are then pre calculated. This gives a good initialization to start with the HAFMM (this method requires the two neighboring grid points to be known for second order accurate propagation). After initialization the algorithm is run until the TOF values at all grid points have been calculated.

This procedure is repeated for all different detector positions, resulting in n different TOF maps. Since the grids of the optical absorption map and the TOF maps are not necessarily the same, we use bicubic interpolation to obtain the TOF values at off grid points.

2.4 Obtaining the speed of sound map

In our algorithm, a speed of sound map has to be known before the optical absorption reconstruction can start. We obtain this speed of sound map indirectly from measurements which are contained in the photoacoustic measurement signals $p(\boldsymbol{r}, t)$. This is possible because we have placed a passive element in our photoacoustic setup, which acts as a ultrasound point source, allowing us to take UTT measurements. Due to the geometrical placement of the passive element opposite to the ultrasound detectors, the generated ultrasound signal does not interfere with the simultaneously generated photoacoustic signals from our object. We have developed a method to obtain accurate projections of acoustic attenuation and (inverse) speed of sound through the object in a maximum likelihood framework[16] from these ultrasound measurements. This method has been further improved and its results will be published elsewhere.

Once the projections of speed of sound and acoustic attenuation are determined, we can proceed with estimating the speed of sound distribution inside the object. The projections of speed of sound are given in the form of a TOF value of path through the object connecting the passive element $\boldsymbol{r}_\mathrm{p}$ with the detector $\boldsymbol{r}_i$:

$$t_f(\boldsymbol{r}_i, \boldsymbol{r}_\mathrm{p}) = \int_{l(\boldsymbol{r}_i, \boldsymbol{r}_\mathrm{p}, c)} \frac{1}{c(\boldsymbol{r})} \mathrm{d}\boldsymbol{r} \tag{8}$$

Here $l(\boldsymbol{r}_i, \boldsymbol{r}_\mathrm{p}, c)$ is the (possibly curved) ray path connecting the passive element with the detector element. Because the path $l(\boldsymbol{r}_i, \boldsymbol{r}_\mathrm{p}, c)$ is dependent on the speed of sound distribution $c(\boldsymbol{r})$ this is a nonlinear problem. It can be iteratively solved in a linear way by using a previous estimate $\hat{c}^{(i)}(\boldsymbol{r})$ to calculate the next estimate $\hat{c}^{(i+1)}(\boldsymbol{r})$. When the ray path is calculated using the previous estimate, the resulting relation is linear.

In order to obtain the path $l(\boldsymbol{r}_i, \boldsymbol{r}_\mathrm{p}, c)$ we will look again at the Eikonal equation:

$$|\nabla t(\boldsymbol{r})|^2 = \frac{1}{c(\boldsymbol{r})^2} \tag{9}$$

where we can set as initial condition $t(\boldsymbol{r}_\mathrm{p}) = 0$. If we use the HAFMM again, we can find the first arrival time solution to this partial differential equation. Given that solution for $t(\boldsymbol{r})$, we can trace the ray path from anywhere in the domain to $\boldsymbol{r}_\mathrm{p}$, via a gradient descent approach. We can see this by realizing that the path from detector location $\boldsymbol{r}_i$ to $\boldsymbol{r}_\mathrm{p}$ is described by the solution to the differential equation:

$$\frac{\mathrm{d}l}{\mathrm{d}\tau} = -\nabla t\Big(l(\tau)\Big) \tag{10}$$

with initial condition $l(0) = \boldsymbol{r}_i$. We solve this equation via the fourth order Runge-Kutta (RK4) method. The RK4 method is iterated, until we are at a predefined distance from the final point $\boldsymbol{r}_\mathrm{p}$. We then step in a straight path from there to the final point in order to avoid strange behavior close to the final point where the gradient of $t(\boldsymbol{r})$ might not be well defined.

For the discretization of this problem, we will use a uniform sampled rectangular grid to hold the speed of sound distribution $c(\boldsymbol{r})$. The values of the the grid points are represented in the vector $\boldsymbol{x}_\mathrm{c}$. These points will contain the inverse speed of sound distributions, thus actually the slowness distribution, which is necessary to make the relation linear. We do not want to reconstruct the whole domain of the ray path, which includes the detector as well as the passive element, but only the part which is occupied by the object. To make the projection correct, we hold in the vector with slowness values $\boldsymbol{x}_\mathrm{c}$ the actual slowness value in the object subtracted with the slowness of the background medium:

$$x_{\mathrm{c},k} = \frac{1}{c(\boldsymbol{r}_k)} - \frac{1}{c_0} \tag{11}$$

The projection measurements (which are also TOF values) are denoted by $\boldsymbol{z}_\mathrm{t}$. For a given ray path, we can describe the linear relation via the matrix operation H_t. This matrix thus dependents on the ray path, so implicitly it is dependent on the initial speed of sound distribution.

$$\boldsymbol{z}_\mathrm{t} = \mathrm{H}_\mathrm{t}(\boldsymbol{x}_\mathrm{c})\boldsymbol{x}_\mathrm{c} \tag{12}$$

Here the notation $\mathrm{H}_\mathrm{t}(\boldsymbol{x}_\mathrm{c})$ stands for the projection matrix created from a given slowness distribution $\boldsymbol{x}_\mathrm{c}$. To solve this problem iteratively, we start with an initial guess of the vector $\boldsymbol{x}_\mathrm{c}^{(i)}$ and calculate a solution to the regularized cost function:

$$\hat{\boldsymbol{x}}_\mathrm{c}^{(i+1)} = \arg\max_{\boldsymbol{x}_\mathrm{c}} \left(||\boldsymbol{z}_\mathrm{t} - \mathrm{H}_\mathrm{t}(\hat{\boldsymbol{x}}_\mathrm{c}^{(i)})\boldsymbol{x}_\mathrm{c}||^2 + \lambda||\mathrm{H}_{\mathrm{G}_\mathrm{x}}\boldsymbol{x}_\mathrm{c}||^2 + \lambda||\mathrm{H}_{\mathrm{G}_\mathrm{y}}\boldsymbol{x}_\mathrm{c}||^2 \right) \tag{13}$$

The same regularization is used here as is explained before in the section on reconstruction of the optical absorption distribution. We solve this iteratively with the LSQR method.

2.5 Reconstructing the acoustic attenuation map

Once the speed of sound map is known, the reconstruction of the acoustic attenuation map is possible. The same ray paths as from the last iteration of the speed of sound reconstruction can be used. The projections that are measured, are projections of the frequency independent attenuation constant α_0 from the frequency dependent attenuation function:

$$\alpha(\omega) = \alpha_0|\omega|^y \tag{14}$$

The projection measurements are related to acoustic attenuation distribution $\alpha_0(\boldsymbol{r})$ via:

$$a(\boldsymbol{r}_i, \boldsymbol{r}_\mathrm{p}) = \int_{l(\boldsymbol{r}_i, \boldsymbol{r}_\mathrm{p}, c)} \alpha_0(\boldsymbol{r})\mathrm{d}\boldsymbol{r} \tag{15}$$

Here we show the attenuation measurement over the path $l(\boldsymbol{r}_i, \boldsymbol{r}_\mathrm{p}, c)$ connecting detector $\boldsymbol{r}_i$ with the passive element $\boldsymbol{r}_\mathrm{p}$. Our maximum likelihood algorithm[16] can be used to extract these projections from photoacoustic signals generated by the passive element. As reconstruction method, we use exactly the same LSQR algorithm as in the final iteration of the speed of sound reconstruction.

3. RESULTS

We validate our approach on computer simulations, because the experimental setup is not yet fully operational.

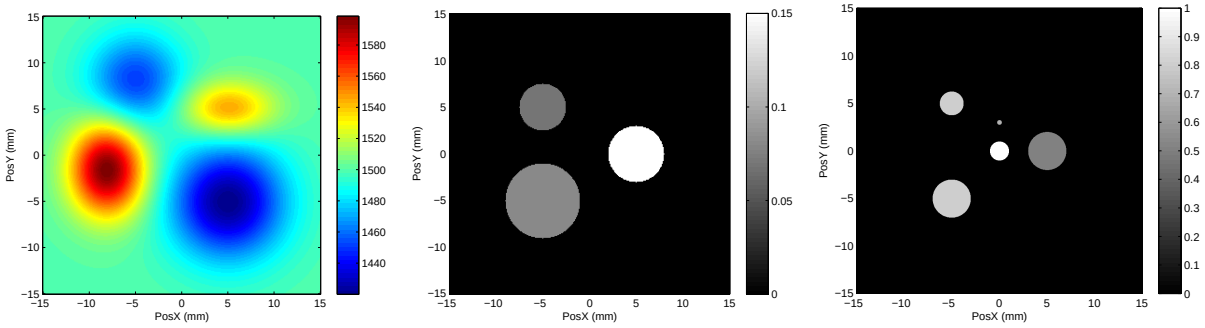

(a) Speed of sound phantom **(b)** Acoustic attenuation phantom **(c)** Optical absorption phantom

Figure 1. Overview of the numerical phantoms used in this study

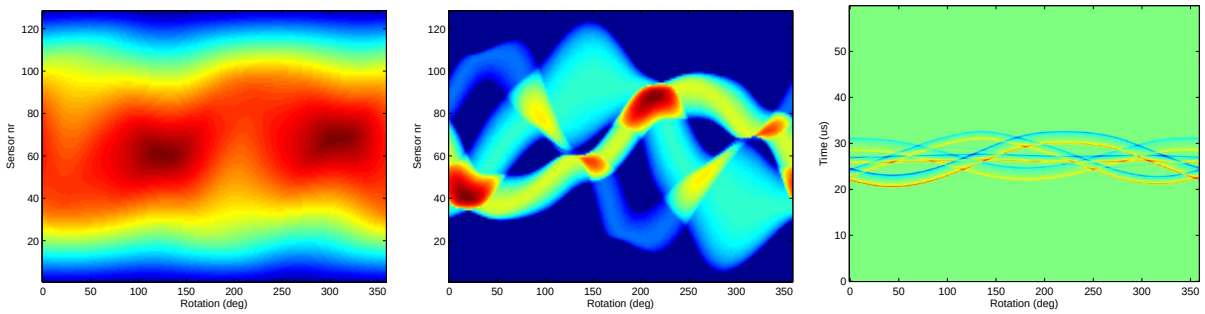

(a) Time of flight sinogram **(b)** Acoustic attenuation sinogram **(c)** Photoacoustic pressure measurements

Figure 2. Sinogram measurements obtained from the numerical phantoms

3.1 The simulation data

The geometrical parameters of our physical experimental setup were used in the generation of simulation data. To generate the measurements, we use high resolution numerical phantoms on which we apply the forward model (2) of the photoacoustic measurements. The numerical phantoms are displayed in Fig 1. For the generation of speed of sound and acoustic attenuation projection measurements, we calculated the ray paths based on the numerical phantom with the HAFMM method. Projections were then obtained by tracing the ray paths over the speed of sound and acoustic attenuation distributions. These result in the sinograms of time of flight and integrated attenuation. The generated sinograms are displayed in Fig.2.

3.2 Reconstructions of the acoustic parameters

To investigate the impact of the curved rays on the reconstructions of the acoustic parameters, we reconstructed the data using a straight ray approach and the proposed bend ray approach. The results of applying both approaches on the speed of sound and acoustic attenuation reconstructions are displayed in Fig. 3.

We can clearly see that using the straight ray approach we are unable to reconstruct both distributions correctly. The acoustic attenuation reconstruction (Fig. 3b) is not anymore recognizable to the original phantom. The speed of sound reconstruction 3a) gives the correct trends, but the shape is very much distorted.

Next we investigated the iterative approach with ray refraction correction. The reconstruction from a previous iteration is now used to calculate the bend rays in the next iteration. The results look very successful. Both the speed of sound (Fig. 3c) and the acoustic attenuation (Fig. 3d) distribution are correctly distributed. Only minor artifacts remain visible in the acoustic attenuation reconstruction. The displayed results were obtained using 15 iterations which were enough for the algorithm to converge to a stable solution.

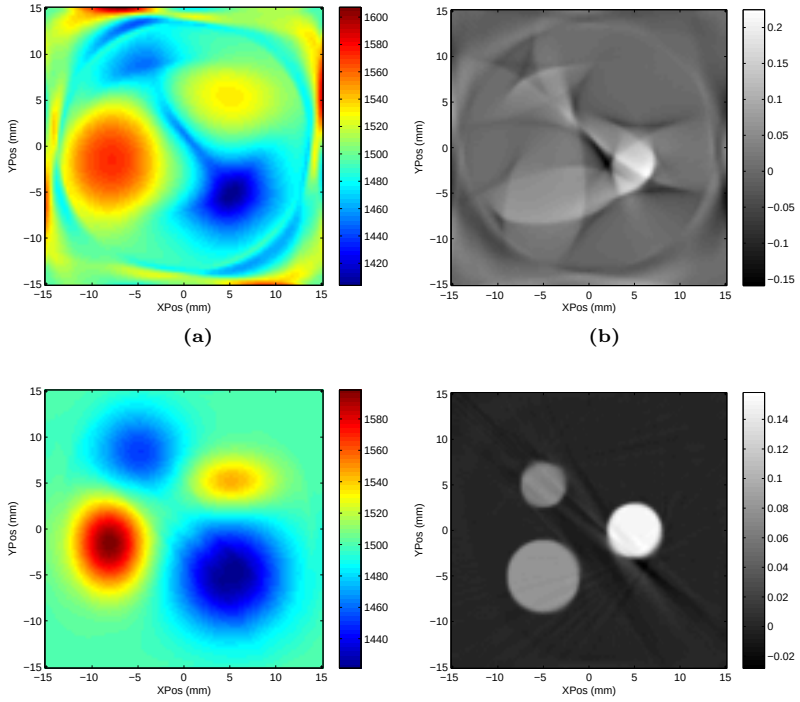

Figure 3. Speed of sound and acoustic attenuation map reconstruction results. The top row show the results of assuming linear propagation of sound rays and the bottom row shows the results of using the iterative correction algorithm with curved rays (15 iterations were used). The images on the left are the speed of sound reconstructions and the images on the right the acoustic attenuation reconstructions.

3.3 Reconstructions of the optical absorption parameters

When the speed of sound distribution was reconstructed, we proceeded with the reconstruction of the optical absorption distribution. Here we use the photoacoustic measurements displayed in Fig. 2c. Different algorithms were tested.

Uniform speed of sound The first algorithm we implemented is based on a constant speed of sound distribution. It does not take into account curved iso-TOF contours. We set the speed of sound equal to 1500 m/s, which is the speed of sound of the background medium. The reconstruction result is displayed in Fig. 4a and a profile plot is displayed in Fig. 4e. We can see that there are blurring artifacts resulting from the incorrect speed of sound assumption. Especially the small structure above the center is distorted.

No speed of sound distribution We implemented the algorithm of Chi Zhang and Wang[8] which does not need an a priori known speed of sound distribution. For the reconstruction, we did not use their modified FBP approach, but used our approach to solve the resulting linear system of equations, which should give better results. The reconstructed image is displayed in Fig. 4b and a profile in Fig. 4f. The reconstructed image still contains artifacts, in fact it is not much better than using the assumption of a uniform speed of sound. The advantage, however, is that no speed of sound value needs to be given to the algorithm, which might not always be known accurately. The authors claim that the algorithm should be able to deal with small speed of sound inhomogenities of up to 10%. This is not true for our simulation study which also has inhomogenities of up to 10%, however the inhomogenities are above and below the background speed of sound. Their algorithm performs better when all inhomogenities are either all above or all below the background speed of sound.

Assuming straight ray propagation To investigate the effect of using straight ray propagation, we used the

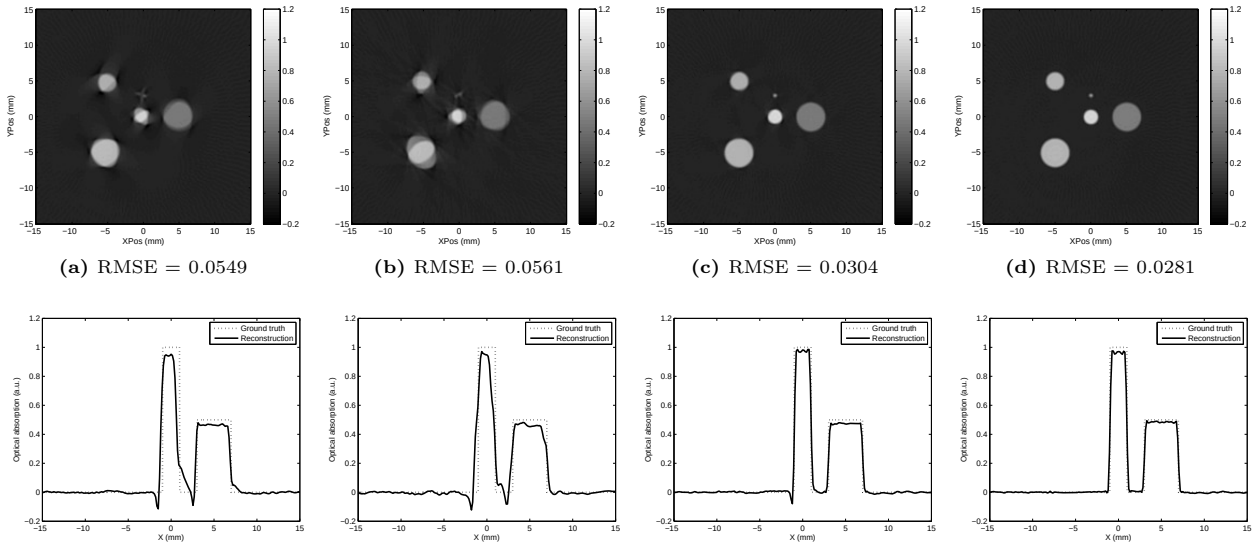

(a) RMSE = 0.0549 **(b)** RMSE = 0.0561 **(c)** RMSE = 0.0304 **(d)** RMSE = 0.0281

(e) **(f)** **(g)** **(h)**

Figure 4. Optical absorption distribution reconstruction results. Shown here are the four different implementations with the corresponding RMSE with respect to the ground truth data. The top row shows the reconstructed images. The bottom row shows profile plots along the horizontal center of the image. (a) and (e): Reconstruction assuming a uniform speed of sound of 1500 m/s. (b) and (f): Reconstruction assuming no sound speed distribution, with the correlation method of Chi Zhang and Wang.[8] (c) and (g): Reconstruction based on straight ray approximations. (d) and (h): Reconstructions using our proposed ray refraction correction method.

straight ray reconstruction result of the speed of sound map. The iso-TOF contours were subsequently calculated by tracing straight rays through the obtained speed of sound map. The obtained linear system was solved and the solution is displayed in Fig. 4c. A profile of the reconstruction is displayed in Fig. 4g. The result is a lot improved compared to the uniform speed of sound reconstruction. The are hardly any artifacts visible anymore and most of the RMSE error is probably due to the limited bandwidth of the reconstructed image.

Assuming bend ray propagation Finally, our proposed method to reconstruct a speed of sound distribution with refraction corrections and using the result with the HAFMM method to calculate iso-TOF curves is tested. The results of the reconstruction are displayed in Fig. 4d and Fig. 4h. The results are artifact free and good reconstructions can be obtained.

4. CONCLUSIONS AND FUTURE WORK

A new method to reconstruct speed of sound, acoustic attenuation and optical absorption distributions from only photoacoustic measurements was proposed. The improvements over other existing methods include the use of ray refraction correction in the speed of sound reconstruction procedure, the way to calculate the iso-TOF contours with the HAFMM algorithm and the fact that no separate UTT measurement is necessary. The performance of the method was verified against three other implementations. The first implementation was based on assuming a known constant speed of sound. The second implementation did not assume any speed of sound distribution and uses a correlation approach to correct for the inhomogenities. The third method does not assume ray refraction and calculates the iso-TOF contours explicitly with ray tracing along straight lines. The main results can be seen in Fig. 4.

Experiments are performed on numerically simulated data and the results indicate that the method performs well. The results are better than the first two implemented methods and slightly better or comparable to the third approach. However, the proposed method is more efficient than the third method in terms of computational

complexity. This is caused by the fact that the TOF values are calculated in a way which only considers each value in the speed of sound grid once per projection.

In the future we plan to do more numerical simulations, we will look at the influence of noise and the influence of using different numerical phantoms. Also we are planning to get our experimental setup operational so that we can verify our method to real physical data.

ACKNOWLEDGMENTS

This research is funded by the Institute of Biomedical Technology (BMTI) of the University of Twente via the NIMTIK program and by a personal grant to one of the authors S.M. in the Vernieuwingsimpuls program by the Netherlands Organization of Scientific Research NWO and the Technology Foundation STW.

REFERENCES

[1] Xu, M. and Wang, L. V., "Photoacoustic imaging in biomedicine," *Rev. Sci. Instrum.* **77**(4) (2006).

[2] Gusev, V. E. and Karabutov, A. A., [*Laser Optoacoustics*], American Institute of Physics (1993).

[3] Anastasio, M. A., Zhang, J., and Pan, X., "Image reconstruction in thermoacoustic tomography with compensation for acoustic heterogeneities," in [*SPIE Medical Imaging 2005*], **5750**, 298–304 (2005).

[4] Jin, X. and Wang, L. V., "Thermoacoustic tomography with correction for acoustic speed variations," *Phys. Med. Biol.* **51**(9), 6437–6448 (2006).

[5] Paige, C. C. and Saunders, M. A., "LSQR: An algorithm for sparse linear equations and sparse least squares," *ACM T. Math. Software* **8**(1), 43–71 (1982).

[6] Jiang, H., Yuan, Z., and Gu, X., "Spatially varying optical and acoustic property reconstruction using finite-element-based photoacoustic tomography," *J. Opt. Soc. Am. A* **23**, 878–888 (April 2006).

[7] Zhang, J., Wang, K., Yang, Y., and Anastasio, M. A., "Simultaneous reconstruction of speed-of-sound and optical absorption properties in photoacoustic tomography via a time-domain iterative algorithm," in [*SPIE Photons Plus Ultrasound: Imaging and Sensing 2008*], **6856**, 68561F–1–68561F–8 (2008).

[8] Zhang, C. and Wang, Y., "A reconstruction algorithm for thermoacoustic tomography with compensation for acoustic speed heterogeneity," *Phyisics in Medicine and Biology* **53**, 4971–4982 (2008).

[9] Manohar, S., Willemink, R. G. H., van der Heijden, F., Slump, C. H., and van Leeuwen, T. G., "Concomitant speed-of-sound tomography in a photoacoustic imager," *Appl. Phys. Lett.* **91**(13), 131911 (2007).

[10] Willemink, R. G. H., Manohar, S., Slump, C., van der Heijden, F., and van Leeuwen, T. G., "Acoustic property measurements in a photoacoustic imager," in [*SPIE Novel Optical Instrumentation for Biomedical Applications*], **6631**, 663109 (2007).

[11] Willemink, R. G. H., Manohar, S., Purwar, Y., Slump, C. H., van der Heijden, F., and van Leeuwen, T. G., "Imaging of acoustic attenuation and speed of sound maps using photoacoustic measurements," in [*SPIE MI 2008: Ultrasonic Imaging and Signal Processing*], McAleavey, S. A. and D'hooge, J., eds., **6920**, 692013 (2008).

[12] Xu, Y. and Wang, L. V., "Effects of acoustic heterogeneity in breast thermoacoustic tomography," *Phys. Med. Biol.* **51**, 6437–6448 (2003).

[13] Sethian, J. A., "Fast marching methods," *SIAM Review* **41**, 199–235 (June 1999).

[14] Li, S., Mueller, K., Jackowski, M., Dione, D. P., and Staib, L. H., "Fast marching method to correct for refraction in ultrasound computed tomography," in [*3rd IEEE International Symposium on Biomedical Imaging: Nano to Macro, 2006*], 896–899 (2006).

[15] Li, S., Mueller, K., Jackowski, M., Dione, D. P., and Staib, L. H., "Physical-space refraction-corrected transmission ultrasound computed tomography made computationally practical.," in [*MICCAI (2)*], Metaxas, D. N., Axel, L., Fichtinger, G., and Szkely, G., eds., *Lecture Notes in Computer Science* **5242**, 280–288, Springer (2008).

[16] Willemink, R. G. H., Manohar, S., Slump, C., van der Heijden, F., and van Leeuwen, T. G., "A maximum likelihood method for obtaining integrated attenuation from ultrasound transmission mode measurements," in [*Acoustics '08 Paris*], (2008).